Experimental Seismic Response of a Resilient 2-Story Mass-Timber Building with Post-Tensioned Rocking Walls

Shiling Pei, M.ASCE[1]; John W. van de Lindt, F.ASCE[2]; Andre R. Barbosa, M.ASCE[3]; Jeffrey W. Berman, M.ASCE[4]; Eric McDonnell, M.ASCE[5]; J. Daniel Dolan, M.ASCE[6]; Hans-Erik Blomgren, M.ASCE[7]; Reid B. Zimmerman, M.ASCE[8]; Da Huang[9]; and Sarah Wichman[10]

Abstract: This paper describes the design, construction, and experimental results of a series of full-scale 2-story mass-timber building shake table tests conducted at the Natural Hazards Engineering Research Infrastructure (NHERI) at the University of California, San Diego large outdoor shake table facility. The building specimen utilized a lateral force-resisting system consisting of two post-tensioned rocking walls made of cross-laminated timber (CLT) panels. The structural system was designed to be resilient with the ability to undergo repetitive testing under strong ground motions without significant damage. The test building had an open floor plan suitable for mixed commercial and residential applications. The CLT floor and roof diaphragm had large cantilevered portions that represented realistic aspect ratios. The building was subjected to a series of 14 earthquake ground motions and pushed to a maximum roof drift of 5%. After completion of the dynamic tests, which included several ground motions at the maximum considered earthquake hazard level, the building was able to recenter with no unintended structural damage, highlighting the resilience of the mass-timber rocking-wall structural system. **DOI: 10.1061/(ASCE)ST.1943-541X.0002382.**

Introduction

Tall buildings ranging from 8 to 20 stories are relatively common in urban areas because they offer a means for developers to balance occupant density and land costs. While traditional light-frame wood construction is not allowed by current building codes in the United States at this height range, a new type of mass-timber construction utilizing heavy timber structural materials, such as glulam and cross-laminated timber (CLT), has emerged in recent years targeting the tall building market. Efforts to introduce such systems in building codes have been underway in the United States (e.g., Building Code Division, State of Oregon 2018) to make tall wood building construction possible. Currently, a number of successful building projects utilizing mass-timber components (CLT and/or glulam, as well as a combination of steel and concrete) around the world (e.g., the 10-story Forte building in Melbourne, Australia; the 14-story Treet building in Norway; the 9-story Stadthaus Building in London; the 18-story Brock Commons building at the University of British Columbia, etc.) have demonstrated the viability and benefit of tall wood construction, which includes a reduction in construction time, reduced demands on foundations, and positive environmental impacts. CLT construction is gaining traction among building owners and investors for tall buildings in large cities, some of which are located in high seismic regions. In areas of high seismicity, reliable and ductile lateral force-resisting systems are necessary, and this new construction type offers an opportunity to incorporate resilient structural engineering concepts at the early stages of system development. Achieving the resilient seismic performance of buildings (i.e., damage free or rapidly repairable), in this case in CLT-based building systems located in areas of high seismicity, can greatly improve community resilience. This potential of improvement in community resilience is the motivation of this experimental study.

The performance of CLT buildings under seismic loading has been studied by researchers around the world since the early 2000s. A number of previous research projects on CLT systems have focused on platform CLT construction in which CLT panel walls have served as both the gravity-bearing system and the lateral system (Pei et al. 2014). Component-level and system-level tests, including a 7-story CLT building shake table test (Ceccotti et al. 2013), were conducted for platform CLT building systems. The results revealed the rigidity of the platform construction style and its vulnerability to large earthquakes due to damage from overturning demands and large accelerations resulting from a lack of softening and energy dissipation (Popovski et al. 2010). While platform construction is suitable for wall-dense floor plans, such as residential buildings, modern mixed-use tall buildings require a more flexible open floor plan and more ductile lateral systems to reduce seismic force demand and acceleration amplification. The experiments and

[1]Associate Professor, Dept. of Civil and Environmental Engineering, Colorado School of Mines, Golden, CO 80401 (corresponding author). Email: spei@mines.edu

[2]George T. Abell Professor in Infrastructure, Dept. of Civil and Environmental Engineering, Colorado State Univ., Fort Collins, CO 80523.

[3]Assistant Professor, School of Civil and Construction Engineering, Oregon State Univ., Corvallis, OR 97331.

[4]Thomas & Marilyn Nielsen Associate Professor, Dept. of Civil and Environmental Engineering, Univ. of Washington, Seattle, WA 98195.

[5]Associate, KPFF Consulting Engineers, 111 SW 5th Ave. #2600, Portland, OR 97204.

[6]Professor, Dept. of Civil and Environmental Engineering, Washington State Univ., Pullman, WA 99164.

[7]Director of Testing and Characterization, Katerra, 542 1st Ave. S, Seattle, WA 98104.

[8]Associate, KPFF Consulting Engineers, 111 SW 5th Ave. #2600, Portland, OR 97204.

[9]Graduate Student, Dept. of Civil and Environmental Engineering, Colorado School of Mines, Golden, CO 80401.

[10]Graduate Student, Dept. of Civil and Environmental Engineering, Univ. of Washington, Seattle, WA 98195.

Note. This manuscript was submitted on May 10, 2018; approved on February 4, 2019; published online on August 23, 2019. Discussion period open until January 23, 2020; separate discussions must be submitted for individual papers. This paper is part of the ***Journal of Structural Engineering***, © ASCE, ISSN 0733-9445.

results presented in this paper are part of a six-university collaborative research project called the Natural Hazards Engineering Research Infrastructure (NHERI) Tall Wood Project funded by the National Science Foundation (NSF), with the objective of developing a resilience-based seismic design methodology for tall wood buildings. The project utilizes large structural testing facilities funded through NSF's NHERI program, including the outdoor shake table at the University of California, San Diego (UCSD) used for the tests described here. The NHERI Tall Wood Project is particularly focused on enabling a more flexible architectural configuration by combining a resilient CLT-based lateral system with a heavy-timber gravity-framing system. This design configuration that separates lateral elements from the gravity system is commonly adopted for concrete and steel high-rise buildings.

Resilient wood lateral force-resisting systems were initially proposed and studied by researchers in New Zealand starting in the early 2000s (Buchanan et al. 2008; Palermo et al. 2005, 2006). Post-tensioning techniques have been applied to wood-frame moment connections and walls (Buchanan et al. 2008; Iqbal et al. 2015, 2016a, b) and used in real building projects (Palermo et al. 2012). The subsequent development of the post-tensioned wood system led to the commercial application of such systems in building projects (Holden et al. 2012). Recently, a reversed cyclic load testing of post-tensioned CLT rocking walls was conducted by Ganey et al. (2017) and modeling parameters were derived from that data by Akbas et al. (2017). The understanding of the rocking timber lateral system obtained from these earlier efforts was applied to the design of the 2-story test building described herein. This test also combined the use of cantilevered diaphragms and a separate gravity-framing system, and represents the largest scale-rocking CLT wall system tested to date.

The objective of the test program presented in this paper was to examine the dynamic behavior of a mass-timber building system with resilient rocking walls at full scale, with details similar to those necessary for implementation in practice. The test also pushed the building system to very large drift levels (beyond current building code permission) in order to validate the robustness of the structural system.

Design Considerations for the Test Building

There are several key components of the test, including: (1) the resilient post-tensioned rocking-wall system; (2) the mass-timber diaphragms with and without composite concrete topping; (3) a shear transfer detail connecting the rocking wall and the diaphragms; and (4) the gravity framing designed using both platform- and balloon-framing details to tolerate large lateral drifts with minimal damage.

An earlier planning study explored the design, modeling, and cyclic loading behavior of post-tensioned rocking walls made from CLT panels (Pei et al. 2014; Ganey et al. 2017; Akbas et al. 2017). During that project, a series of reverse-cyclic loading tests were conducted at Washington State University on full-sized rocking walls (Ganey et al. 2017), and the numerical models for the rocking-wall component were developed (Akbas et al. 2017). Through these earlier investigations, it was discovered that CLT rocking walls have the potential to remain essentially damage free and fully self center at interstory drifts of up to 5%, and sustain only limited crushing damage at the bottom corners (i.e., the toes) of the panels at drift ratios near 10%, if designed appropriately. Further, the system could be designed such that the lateral resistance does not decrease significantly at these large drift levels. Notably, these low-damage characteristics were achieved at drift levels far beyond the current codified seismic drift requirements (i.e., 2.5% drift under the design level earthquake loading).

The geometry of the test specimen was determined based on several factors, including the desired diaphragm aspect ratio, the need for an open floor plan, and the limitations of the shake table at the shared use facility at the University of California, San Diego (NHERI at UCSD). A 2-story building system was designed for this stage of the research to inform future analysis and testing of taller structures. At the beginning of the NHERI TallWood Project, the researchers, in collaboration with an advisory team of architects and structural engineering practitioners, evaluated the potential market for tall wood buildings, which pointed toward mixed-use buildings with open floor plans that can be reconfigured through nonstructural walls. In this test, two diaphragm designs with different CLT panel and glulam beam grid arrangements were investigated, including one with composite concrete topping and the other with CLT only. Because the CLT floor needs to satisfy deflection and vibration requirements (the strength of the CLT floor in bending typically does not control the design), the clear span of a CLT-only floor is limited. With a glulam beam grid under the CLT floor, the span of the CLT-only floor diaphragm is 3.05 m (10 ft). The roof diaphragm consisted of a concrete-CLT composite system (with 5-ply CLT) that spanned 6.10 m (20 ft). The design of the untopped CLT floor diaphragm and the sizing of the chord connectors (custom-made steel straps) over panel splices were conducted in accordance with the principles of mechanics, using values of fastener and member strength in accordance with test results available in the literature and the US 2015 National Design Specification (NDS) for Wood Construction. The design of the concrete-CLT composite roof diaphragm was conducted based on earlier testing of similar composite floors at Oregon State University (Higgins et al. 2017; Johnson 2017) and basic principles of mechanics. In addition, the fasteners used in the floor and roof panel joints, such as the spline joints and floor-to-beam fasteners, were not used to meet requirements for the continuity of diaphragm tension chords.

In order to accommodate the large interstory drift, the gravity-framing connections were designed to rock at the beam-to-column interface (i.e., the gravity frame is not part of the lateral force-resisting system). Additionally, a combination of platform- and balloon-framed columns (i.e., discontinuous and continuous at the first floor) were used to investigate the feasibility of connections for both framing methods. For platform-framed column-beam joints, modified standard Simpson Strong-Tie column caps were installed with slotted bolt holes to allow joint rotation. For the balloon-framed columns, a custom-designed paired-beam seating connection was utilized at 2-story continuous columns. The connection details were inspired by a design by KPFF Consulting Engineers, an industry partner on the NHERI TallWood Project, for the proposed Glenwood CLT Parking Garage project in Springfield, Oregon and the proposed Framework project (Zimmerman and McDonnell 2018) in Portland, Oregon. These connections permit the shear transfer of diaphragm forces during the simultaneous uplift of the CLT rocking walls.

Details of the Test Building Design Configurations

Gravity Framing

As shown in Fig. 1, the test building had a symmetric design with an overall footprint of 6.10 × 17.68 m (20 × 58 ft). The floor elevation was 3.66 m (12 ft) from the foundation and the roof height was 3.05 m (10 ft) from the first floor. The total roof elevation was equal to 6.71 m (22 ft). The post-tensioned rocking walls were balloon framed and extended above the roof diaphragm to allow the installation of a steel saddle utilized for anchoring the post-tensioning

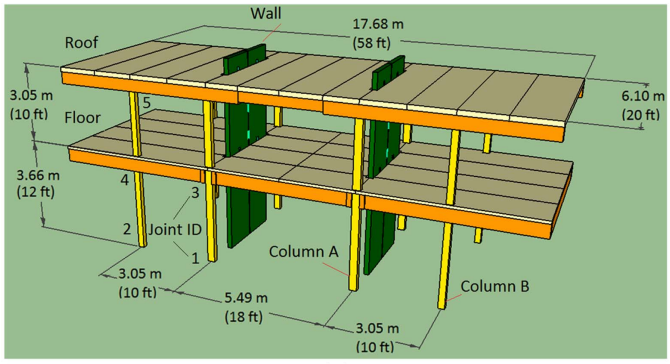

(a)

(b)

Fig. 1. Test building configuration: (a) solid model and dimensions; and (b) photo of the constructed building.

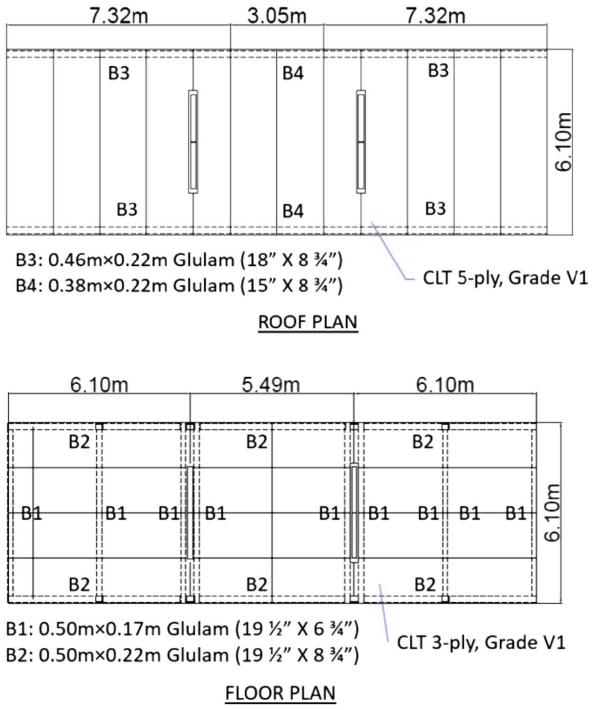

Fig. 2. Layout of the CLT panel and glulam beams for the floor and roof.

(PT) bars. There was a total of eight columns supporting the gravity load of the structure. The four columns close to the center of the building were continuous through the diaphragm, while the others were separated by the floor diaphragm. These two column types are denoted as A and B in Fig. 1. Three types of beam-column joints and two types of column-base connections were used as indicated in Fig. 1. The layout of the CLT panels and the glulam beams for the floor and roof diaphragms are illustrated in Fig. 2. The gravity design of the frame and CLT floor and roof was based on an approximated mass of 321 kg/m^2 (64 psf) for the floor and 386 kg/m^2 (79 psf) for the roof. These weight values were estimated from the as-designed self weight of the structural elements plus the typical weight of the partition [49 kg/m^2 (10 psf)] and miscellaneous secondary finishing items [68 kg/m^2 (14 psf)]. The CLT panel joints were constructed following typical CLT top spline floor splice details with prerouted panel edges covered with plywood strips. The floor and roof diaphragms were designed to be damage free under the planned seismic excitations. A shear demand calculation was conducted to determine the number of structural screws (Simpson Strong-Tie 0.22 × 3–3/8) needed for shear transfer across the panel splices. The chord tensile forces in the diaphragm were carried over panel joints using custom-sized metal straps installed using screws (Simpson Strong-Tie × 3−1/2).

Fig. 3 shows the schematics of the typical gravity-frame beam-column joints used in the test specimen (see Fig. 1 for the joint ID numbers). Most of the connections utilized commercially available connectors with some modifications to accommodate joint rotation during earthquakes. Connector bolt holes were slotted in the vertical direction so that the gravity frame would not engage in moment transfer, thus minimizing damage to columns and joints under large lateral drifts. A consideration of joint fire protection was not incorporated into these details as that was outside the scope of this study.

CLT Rocking Walls

There were two sets of coupled CLT rocking walls installed in the test specimen, as shown in Fig. 1. The walls were coupled using U-shaped flexural steel plate (UFP) energy dissipaters. Similar energy dissipaters were used in the concrete rocking-wall systems (Priestley et al. 1999; Johnston et al. 2014), as well as the CLT rocking walls tested by Ganey et al. (2017). The walls and UFPs were designed using the following process:

1. The wall dimensions and initial PT force were selected to meet the seismic demands computed per ASCE 7-10 (ASCE 2010) for a Class B soil site in San Francisco with an assumed seismic force reduction factor, R, of 6 and using the approximate period per ASCE 7-10. The limit state of wall decompression (initial uplift) was used for this design load.
2. The monolithic beam analogy (Palermo et al. 2012) was used to estimate the strain and stress distribution along the rocking interface of the panel for a given drift. The strain at the extreme outer fiber determined from the monolithic beam analogy was then compared to a crushing strain limit of 0.0056 that was based on panel compression tests for similar material. The design was constrained such that the strain at the outer fiber did not exceed the crushing strain until after 2% drift. It is conservative to use strain at the extreme outer fiber as the limit state because some distribution of crushing along the panel is likely to be acceptable. However, no data exists to set a limit for an acceptable length over which crushing can occur.
3. The U-shaped steel yielding elements were designed to provide a minimum energy dissipation ratio, β, of 0.4, consistent with the recommendations of Sause et al. (2010).

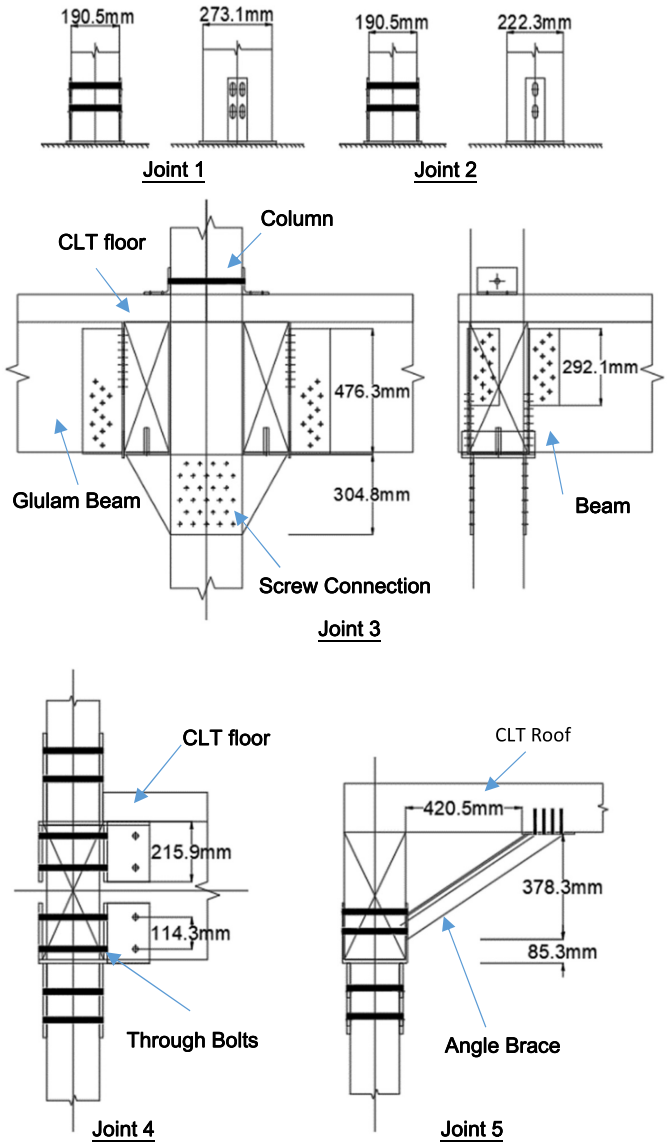

Fig. 3. Gravity frame joint design details.

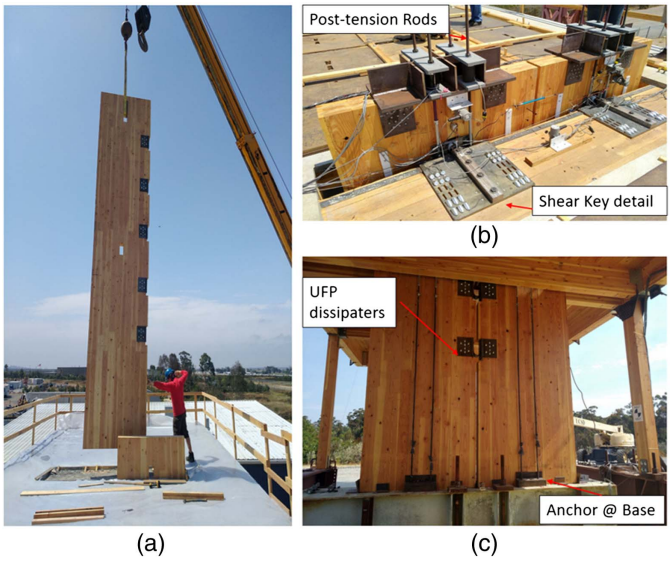

Fig. 4. CLT rocking-wall installation and details: (a) installation of the CLT panel; (b) details on the top of the wall; and (c) details at the base and first story.

4. The post-tensioning bars were checked to ensure that: (1) yielding did not initiate until after both 2% drift and the CLT panel reached the crushing strain at the outer fiber, and (2) the post-tensioning was sufficient to recenter the wall after cycles at 2% drift given the resisting forces of the U-shaped yielding elements.
5. The complete moment-drift response for the wall was determined using the monolithic beam analogy, including the additional moment from the plastic capacity of the U-shaped yielding elements. The forces at the diaphragm locations at 4% drift were then estimated assuming an ASCE 7 load distribution for the design of the diaphragm-wall connection.

The design of these walls was identical. Each had two 1.52 × 7.32 m (5 × 24 ft) CLT panels with a 25-mm gap between them connected by five UFPs. Because the relative location of the UFP elements along the height of the wall does not significantly affect their performance since this is a low-rise and first-mode-dominated structure, they were approximately evenly spaced along the height of the wall, while avoiding the locations of the floor and roof diaphragms for ease of installation. The UFPs were also intentionally placed away from the bottom of the CLT panel so that they were far from the potential crushing zone. As a result, two of the UFPs were located below the CLT floor and three were above it (Fig. 4). The UFPs were connected to the wall panels with high-strength self-tapping timber screws [SWG Schraubenwerk Gaisbach GmbH, (ICC 2018)] installed at 45° into the side of the CLT wall panels (with 45° wedge washers) in order to minimize slip. The rocking walls were post-tensioned externally from the top of the wall to the shake table via a steel box beam. Each panel had four external post-tensioned steel rods placed symmetrically at the center of the wall panel (two each side). A steel saddle detail was installed on the top of the panel to anchor the post-tensioned rods (Fig. 4). The post-tensioned rods were Simpson Strong-Tie 19 mm (3/4″) fully threaded high-strength rods with a yield strength of 634 MPa (92 ksi) and an ultimate strength of 827 MPa (120 ksi) (model numbers ATS-HSR8 and ATS-HSR10). The initial post-tension force (PT force) was 53.4 kN (12 kips) per bar. The force was small enough (40% of the bar yield force 134 kN) to be achieved by manually tightening the anchoring nuts while recording the applied force using load cells. After initial post-tensioning, the loads in each rod were monitored throughout the test program and adjusted to the design value as needed, which was only necessary after a few of the large seismic tests. The monitoring of the bar forces indicated that there was negligible post-tension loss during the relatively short duration of the test program. However, the long-term post-tension force loss in mass-timber buildings would typically need to be closely monitored over a longer duration. The CLT rocking walls were designed to be independent of the gravity frame and engaged only under lateral loads. The CLT walls were dropped into the building through a precut slot in the diaphragm after the gravity frame and floor and roof diaphragms were constructed (as shown in Fig. 4.)

Wall-to-Diaphragm Connection

The rocking-wall lateral system was connected to the diaphragm using the details shown in Fig. 5. The design of the connection ensured effective shear force transfer between the diaphragms and the rocking shear walls, while allowing uplift of the wall panel relative to the diaphragm and providing out-of-plane bracing of the wall. As shown in the figure, a dowel-type steel shear key was inserted into a vertically slotted hole in order to allow the uplift of the rocking wall while transferring lateral loads. The shear key was fabricated with rounded edges to accommodate the rocking motion.

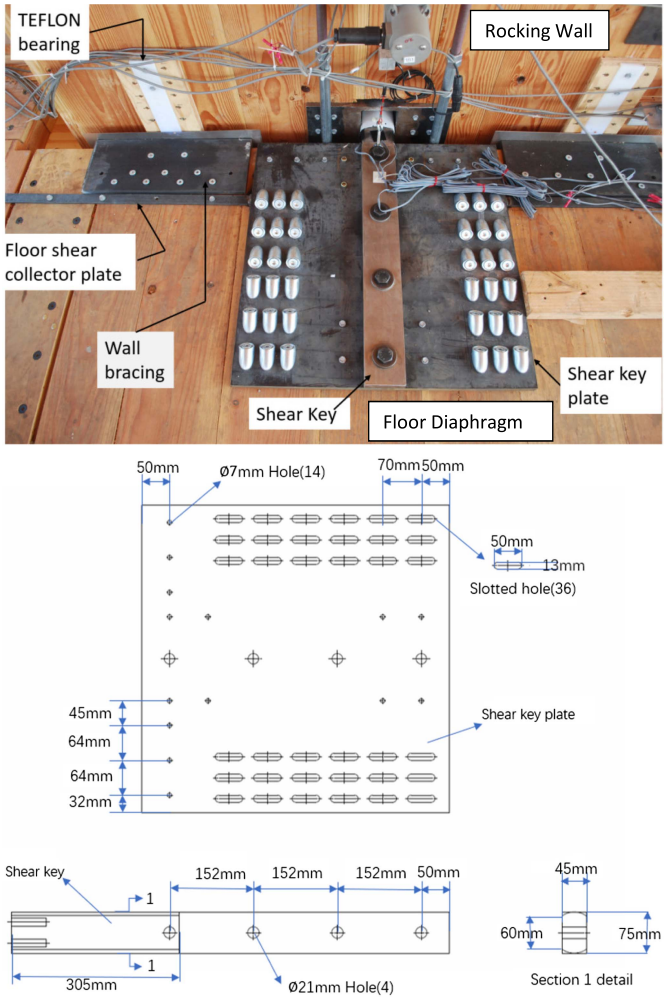

Fig. 5. Shear key connection details between rocking wall and floor diaphragm.

The size and connection of this shear key were designed based on the estimated rocking-wall capacity at 4% drift with an additional safety factor of 1.5. Several steel angles were installed to the diaphragm to provide out-of-plane bracing of the wall. In order to limit the potential for friction at the interface with the wall, a low-friction bearing interface was used between the angle and the wall. To represent the worst-case scenario for the shear keys, they were designed to be cantilevered off the diaphragm on one side of the wall (i.e., simulating the condition if the walls were placed at the building's exterior). This resulted in larger shear keys and connections relative to those needed for the case of the shear key connected to the diaphragm edges on each face of the wall panels.

The load from the shear key was transferred into the diaphragm through a combination of a thick steel plate that was attached to the CLT floor with 45° timber screws (SWG) and steel collector straps welded to the thick plate and ran the full width of the diaphragm, parallel to the walls.

Additional Building Design and Construction Considerations

The roof of the test building was designed as a composite concrete-CLT system. The shear transfer between the 57.2-mm (2.25-in.) concrete topping to the 5-ply CLT was achieved using Simpson Strong-Tie SDWH wood screws (8 in., 0.276″ diameter) installed at 45° and protruding from the CLT floor by approximately 34.9 mm (1−3/8 in.). These shear studs were designed to ensure composite action between the concrete and CLT in order to handle the increased span. As shown in Fig. 6, the concrete topping is reinforced for shrinkage cracks.

The design of the structure was based on the typical dead and live load condition of a mixed-use office building. Because the building was not finished with nonstructural components, the dead weight of the CLT material and the concrete topping was not adequate to achieve the intended design seismic mass. Additional seismic masses were added to the floor in the form of steel trench plates. Each trench plate was approximately $1.22 \times 2.44\ \text{m} \times 25\ \text{mm}$

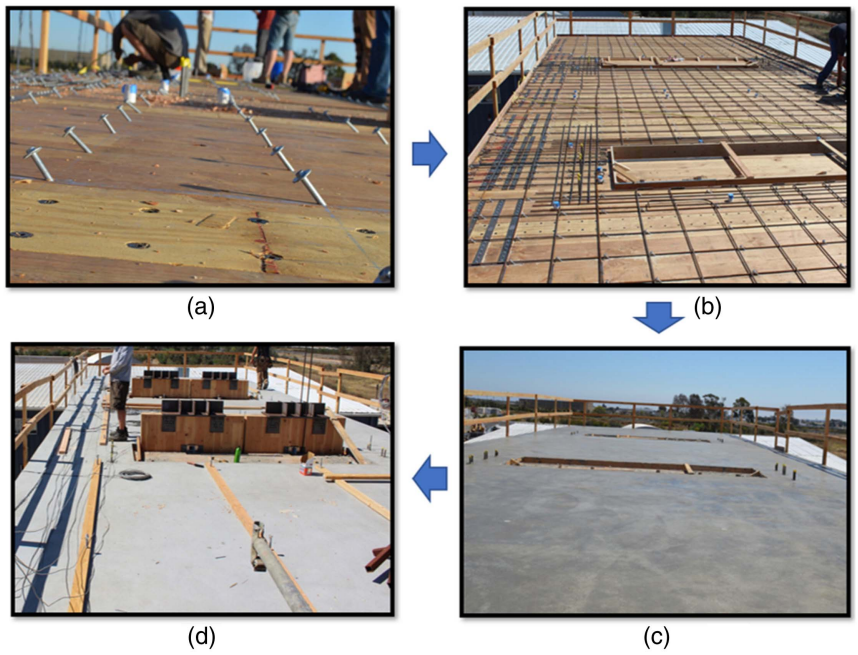

Fig. 6. Construction of the wood-concrete composite roof diaphragm: (a) screw on CLT for shear transfer; (b) rebar for concrete layer; (c) newly poured concrete floor; and (d) completed roof with rocking walls in place.

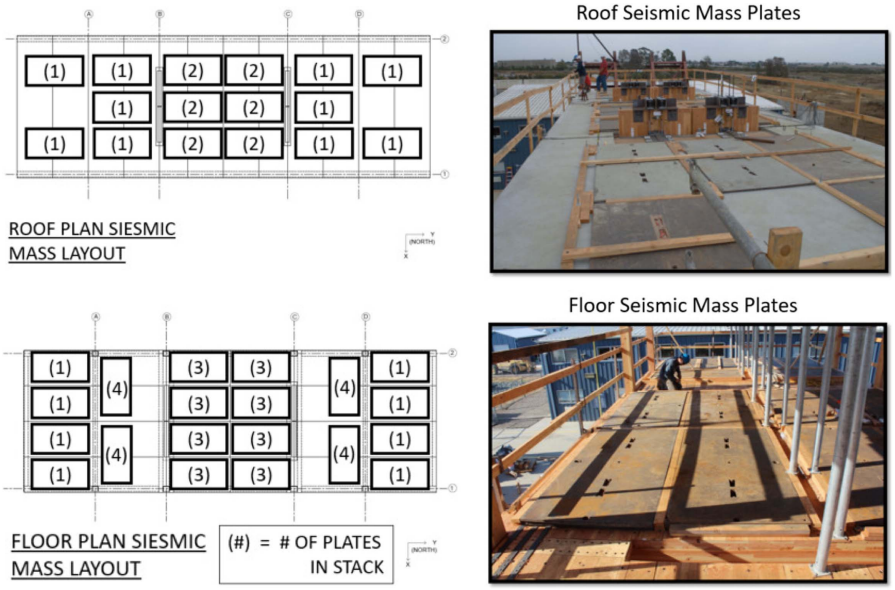

Fig. 7. Arrangement of the additional seismic mass on the roof and floor.

(4 ft × 8 ft × 1 in.) and weighed about 7.1 kN (1.6 kips). A total of 48 plates was added and secured on the floor diaphragm, and 22 were added on the roof to bring the total mass to the aforementioned design values. The plates were secured to the floor using a grid built by dimensional lumbers, which is a technique used previously in large-scale testing programs (van de Lindt et al. 2010, 2013). To avoid artificially strengthening the diaphragm, the wood-grid blocking was cut across the diaphragm splices. Fig. 7 illustrates the arrangement of the seismic mass on the floor and the roof.

The CLT material used in this study was provided by a US CLT manufacturer [DR Johnson Lumber (APA 2018a)] certified as Grade V1 based on APA standard PRG320 (APA 2018b) for CLT panels. The CLT floor level consisted of 3-ply panels and the roof and rocking-wall panels were 5-ply panels. The glulam beams and columns were provided by the same manufacturer with a minimum of 24F-V4 grade for beams and L2 grade for columns.

The installation of the test building was completed in a relatively short period of time (compared to cast-in-place concrete construction) because of the high level of prefabrication of CLT. The gravity frame was finished in four days, including adding the steel plate mass on the floor level. The concrete work for the composite roof took one week to complete. Finally, the rocking walls were installed and post-tensioned in two days. The entire construction took only two weeks despite delays in the shipment of miscellaneous connections and custom steel parts. This time line highlighted the efficiency of prefabricated construction using CLT. A brief outline of the major construction stages is provided in Fig. 8.

Testing Program

The main objective of the testing program was to validate the resilient performance of the post-tensioned CLT rocking-wall lateral system at different levels of seismic intensity. This study was also intended to generate a benchmark dataset for the dynamic responses of a mass-timber diaphragm and gravity frame. These test objectives were achieved through 14 seismic tests conducted at different intensity levels and a systematically implemented instrumentation plan containing over 350 channels of measurement. A variety of sensors were installed on the test building, providing measurements of force, displacement, strain, and acceleration. However, some of these sensors (especially strain gauges placed under the concrete slab) were damaged during the construction of the test specimen and did not record data. There were 46 displacement and acceleration sensors installed on the building frame to obtain the global building response, such as the interstory drift, torsional responses, and floor and roof accelerations. The rocking walls were instrumented with 62 displacement and strain sensors and load cells to measure post-tensioning force, rocking uplift displacement, and CLT panel deformation. A total of 131 sensors (mostly strain gauges on steel reinforcement and chords and displacement sensors between wood-concrete interfaces) was included on the diaphragm for panel deformation, concrete-wood slip, and chord forces. There were 24 strain gauges attached to shear keys to monitor dynamic shear forces during the tests. Some examples of the sensor installations are shown in Fig. 9.

The test building was subjected to a total of 14 earthquake excitations selected to represent three hazard levels for the San Francisco site described in the preceding text: (1) service-level earthquake (SLE, i.e., 50% probability of exceedance in 50 years), (2) design-basis earthquake (DBE, 10% probability of exceedance in 50 years), and (3) maximum considered earthquake (MCE, 2% probability of exceedance in 50 years). Ground motion records from past California earthquakes were used with different scaling factors to match the response spectrum value at the approximate natural period of the 2-story wood building estimated using the empirical formula in ASCE 7-10. During public tests (Tests 6 and 8), which occurred on different days, the unscaled ground motion from the Northridge earthquake (Canoga Park Station Record) was run twice without stopping in between. The objective of these particular tests was to illustrate the ability of the building to withstand multiple consecutive strong earthquakes without the need for repair in between. The shake table at the NHERI at UCSD site is a uniaxial shake table and thus all ground motions were applied in the short direction of the building (i.e., the direction of the CLT rocking walls). The sequence of the tests and the actual peak ground acceleration (PGA) measured from the shake table are presented in Fig. 10. Also shown in the figure is the spectral acceleration of the actual test motions at 0.9 s, which is the approximate first-mode elastic period of the test building based on the white noise excitation test results. The response spectrum of the measured table

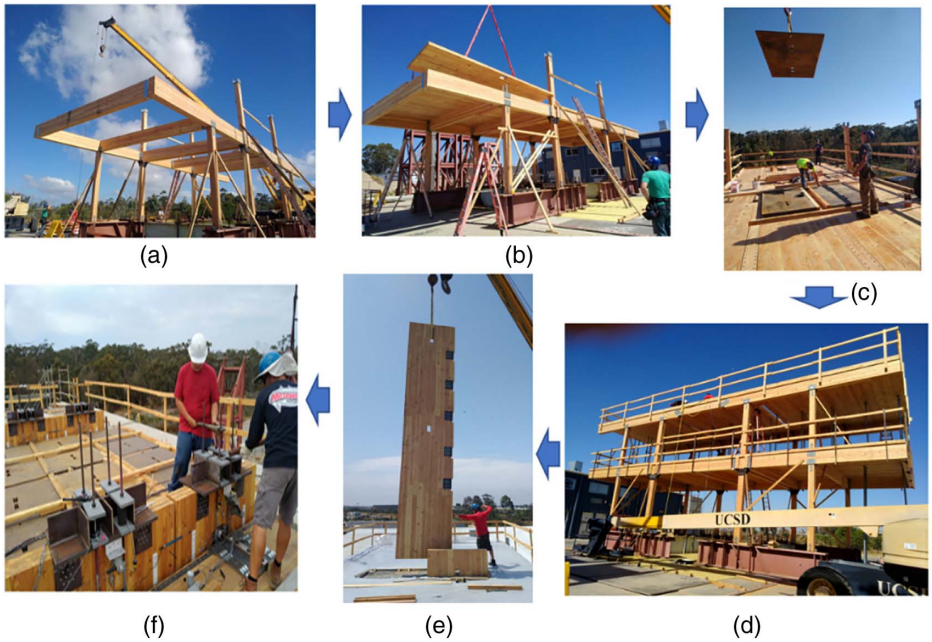

Fig. 8. Construction of the test specimen (concrete placement on roof not shown): (a) gravity framing; (b) floor panel; (c) supplemental seismic mass; (d) completed gravity system; (e) inserting rocking-wall panel; and (f) post-tensioning.

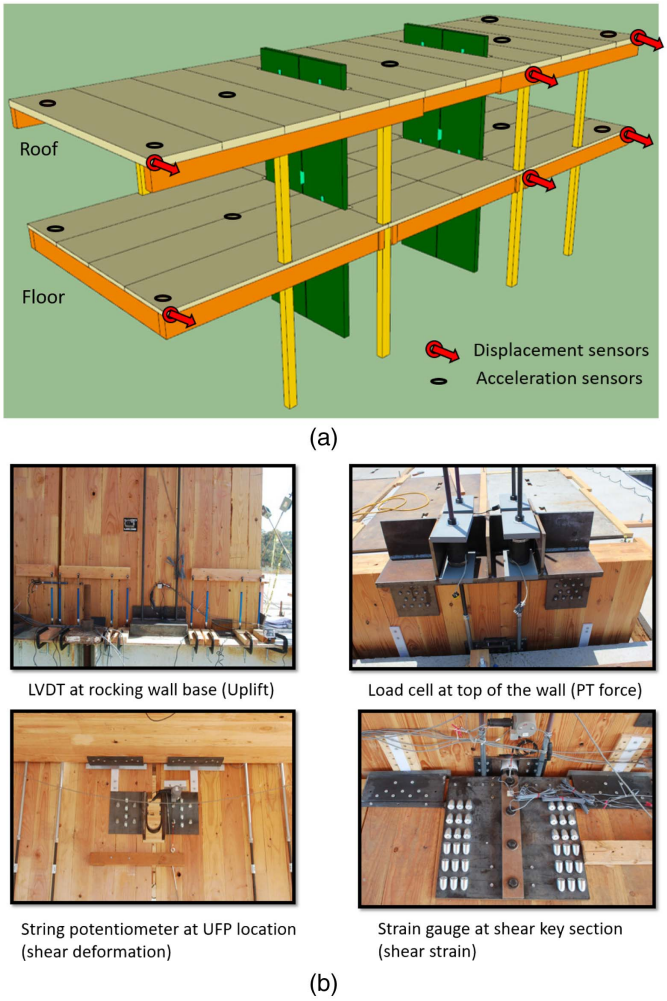

Fig. 9. Installed instrumentation: (a) global displacement and acceleration; and (b) photos of sensors at different components for localized responses.

ground motions is plotted in Fig. 11, which represents the actual seismic excitation experienced by the test building.

Test Results

Global Building Responses

The peak building displacements at the roof and floor levels (relative to the shake table) were calculated using the average of three string potentiometer readings at each level. Fig. 12 illustrates the peak building deformations for the floor and roof. The maximum roof response among all seismic tests was about 350 mm, which corresponds to an approximately 5% overall building drift ratio. As shown in Table 1, the maximum drifts were similar for the upper and lower floors, indicating that the building's lateral response was dominated by a linear first mode for all tests, as was expected for a relatively rigid rocking-wall system. The time-history response of the roof and floor are plotted in Fig. 12 for different selected intensity levels. It is evident that the building had very little residual deformations at all levels of shaking, even for ground motions with MCE-plus intensities, such as Test 14 that corresponds to the ground motion scaled to exceed the MCE level intensity in order to examine the building response under very large deformations. Damage inspections after each earthquake also indicated that there was no structural damage that required repair in any of the tests, except for retensioning of the PT bar, which is discussed in the subsequent text.

The building was subjected to white noise excitation before and after each test to obtain its initial natural period. When there was significant pretension force loss of more than 4.4 kN (1 kips) in the post-tensioned rods after large intensity tests, the post-tensioned rods were retensioned. White noise tests were also conducted to monitor potential building period changes before and after retensioning. The input white noise excitation had a PGA of 0.03 g and a duration of 2 min. The natural periods calculated from all white noise tests are shown in Fig. 13 along with the seismic test maximum roof drifts in order to show the relative test sequence of the

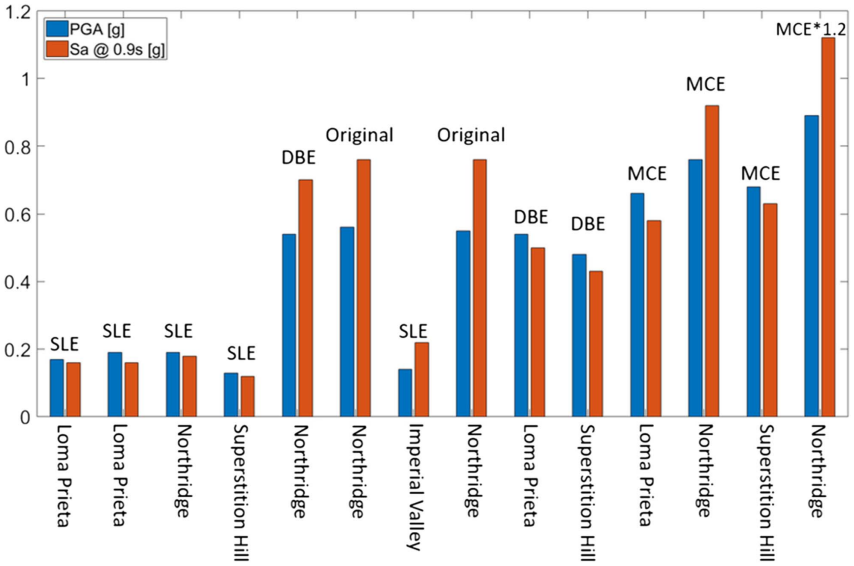

Fig. 10. Ground motions used in the test program.

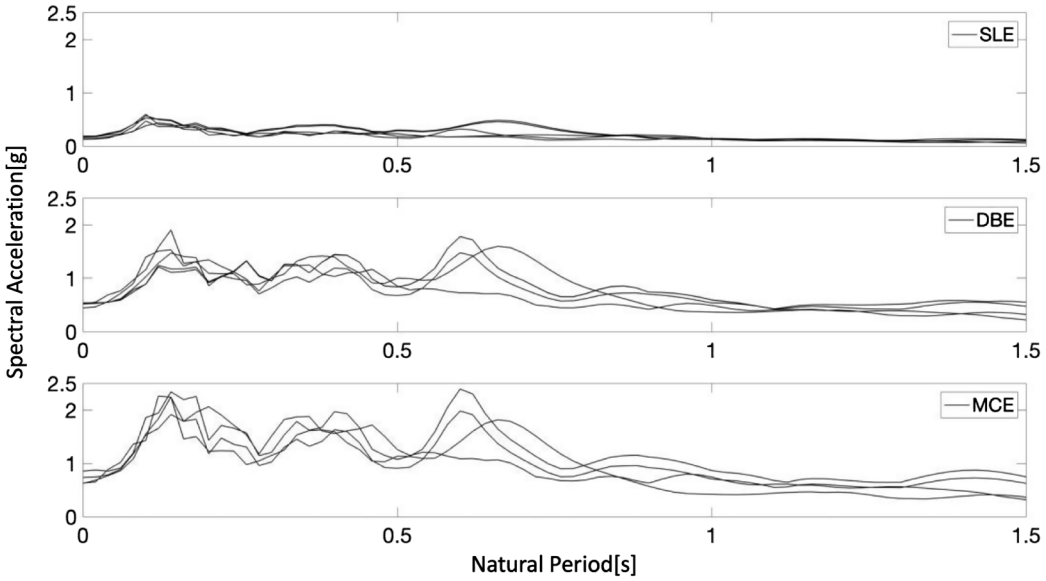

Fig. 11. Spectral acceleration of the ground motion inputs measured on the shake table. (Adapted from Pei et al. 2018.)

white noise tests to seismic tests. The natural period of the building ranged from 0.7 to 1.0 s, which is relatively long for a 2-story building. This data indicates that low-level ground motions have little impact on the building's natural period. However, the elastic period of the building is affected when there is a large event that causes PT force loss (e.g., change between WN20 and WN21 tests) or other minor change to the system, such as the loosening of various screw connections. It is important for designers to consider these changes in the building's natural period when evaluating building safety for aftershock conditions. The loss of post-tensioning force should be repaired as soon as possible for post-tensioned rocking-wall systems following a large earthquake.

From the ground motion response spectra plots shown in Fig. 11, one can obtain the response spectrum value at around 0.9 s and compare it to the measured acceleration of the floor and roof. There were multiple accelerometers attached to the floor and roof level in the direction of the earthquake excitation. The average values of these accelerometers were calculated to represent the average floor and roof acceleration during the tests. The maximum average acceleration measured from each test was plotted in Fig. 14. One can see from these test results that the building system amplified ground acceleration for low-level excitation tests. For large earthquakes, the amplification was not as significant.

The base shear was estimated by multiplying the roof and floor seismic masses with the acceleration time history of the floor and roof found using the average value of the accelerometers installed at these levels. Examples of global building hysteresis (the total base-shear versus roof displacement) for different intensity levels are plotted in Fig. 15. The maximum base-shear forces calculated based on the measured acceleration are also shown for all tests. The hysteresis curves revealed that the building response is nearly linear at low-level ground motions, while it is also shown to be able to

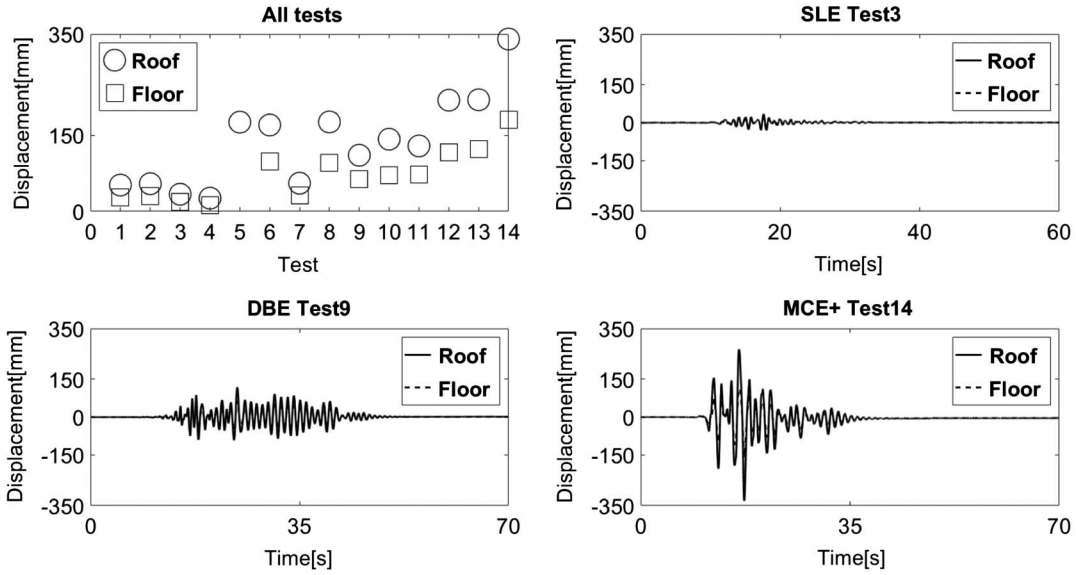

Fig. 12. Peak global displacement responses and example time-history plots.

Table 1. Peak displacements relative to ground and the linear displacement distribution mode

Test ID	Peak roof displacement (mm)	Peak floor displacement (mm)	Peak upper-level drift ratio (%)	Peak lower-level drift ratio (%)	Ratio of drift ratios[a] (upper/lower)
1	52	28	0.80	0.77	1.03
2	55	30	0.83	0.83	1.00
3	34	19	0.56	0.51	1.10
4	26	12	0.47	0.34	1.40
5	176	N/A[b]	N/A	N/A	N/A
6	171	99	2.56	2.71	0.94
7	56	32	0.86	0.87	0.99
8	176	96	2.63	2.63	1.00
9	111	63	1.59	1.73	0.92
10	142	71	2.40	1.94	1.24
11	129	72	1.83	1.97	0.93
12	219	116	3.39	3.17	1.07
13	220	122	3.29	3.34	0.98
14	340	181	5.23	4.94	1.06

[a]If the building displacement is linear along the height, the ratio is 1.0 (i.e., same drift ratios for all stories).
[b]Floor displacement instrumentation malfunctioned during this test.

dissipate energy through hysteretic damping in larger earthquakes. The overall hysteretic energy dissipation is a reflection of many contributors, mainly including the yielding of UFP connectors, friction between different parts of the building, impact of the rocking-wall corners on the foundation, and damage to different components (although this damage might not be visible during inspection). These response characteristics under different ground motion intensities also provided a likely explanation for the acceleration amplification trend revealed in Fig. 14.

Post-Tensioned Rocking-Wall Response

The PT forces were monitored during all tests using load cells. The maximum, minimum, and residual (RES) PT forces during each test are plotted in the first plot of Fig. 16. As examples for different intensity levels, the time-history plots of selected PT bars are also shown. For some PT bars, the post-tension loss was significant during large earthquakes. The MCE-plus test (Test 14) resulted in a tension force loss of about 37 kN, so the residual force was measured as approximately 16 kN following the test, dropping from the initial PT force of 53.4 kN. This PT force drop was mainly caused by the yielding of the bar (i.e., the maximum PT force recorded by the load cell was about 150 kN, while the theoretical yielding load of the PT bar was only 134 kN). The tension force loss was found for only a few PT bars (while the others did not experience significant loss). Thus, the building was able to recenter with negligible residual drift even for these large events. As previously mentioned, the retensioning of the PT bar was conducted if the PT force of the bar was reduced by more than 4.4 kN (1 kip), which corresponded to an approximately 8% loss.

The uplift of the rocking-wall corners and the relative displacement of the coupled rocking-wall panels along their edges (i.e., the approximate shear deformation of the UFPs) were also measured during the tests. These measurements were important for the modeling of the rocking wall as they revealed the kinematics of the rocking behavior. The maximum uplift and relative displacement observed during each test are shown in Fig. 17. The figure also shows the time-history samples from selected tests at different intensity levels. The uplifts and interpanel shear deformation observed on the same panel during the tests were strongly correlated to each other. The time-history data show that the uplift at the panel toe matched the positive portion of the shear deformation very well. This indicates that the rocking-wall panels behaved in a nearly rigid manner during the rocking motion.

The panel uplift can be used to estimate a base rotation angle, which is computed by dividing the uplift by the width of the panel, that can be compared to the building drift. For rigid panels that rock perfectly on a panel toe, the base rotation would be equal to the drift ratio. For deformable panels where a compression zone extends over a width of the panel base, the base rotation computed using the full panel width would be less than the drift ratio. Table 2 compares the rigid body rotational drift to the measured overall roof drift (roof displacement divided by roof height). The rigid body rotation drift was calculated based on the measured panel toe uplift and interpanel UFP shear deformation divided by the panel width.

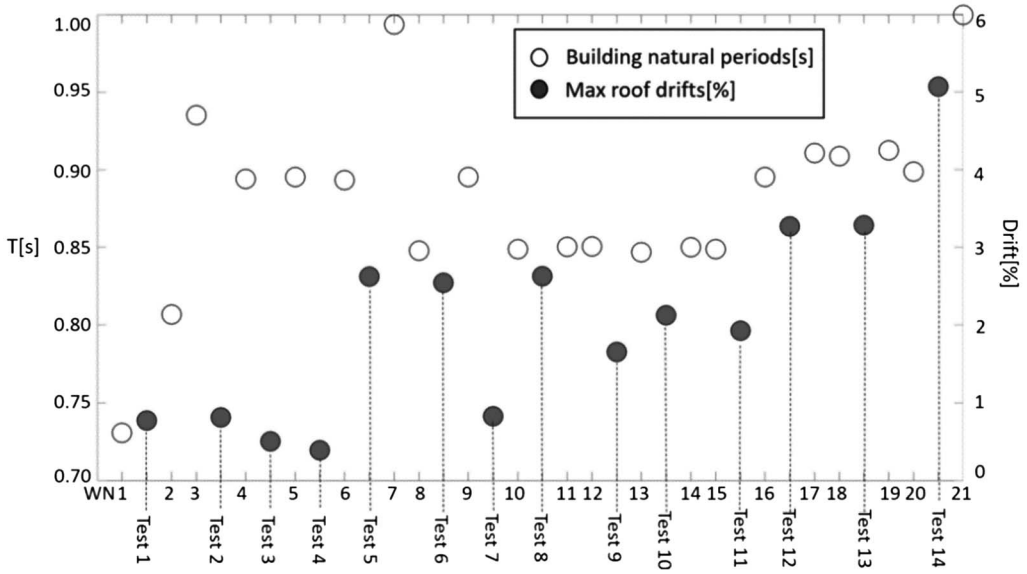

Fig. 13. Peak roof drift ratio from seismic tests and building natural period estimated from white noise (WN) tests.

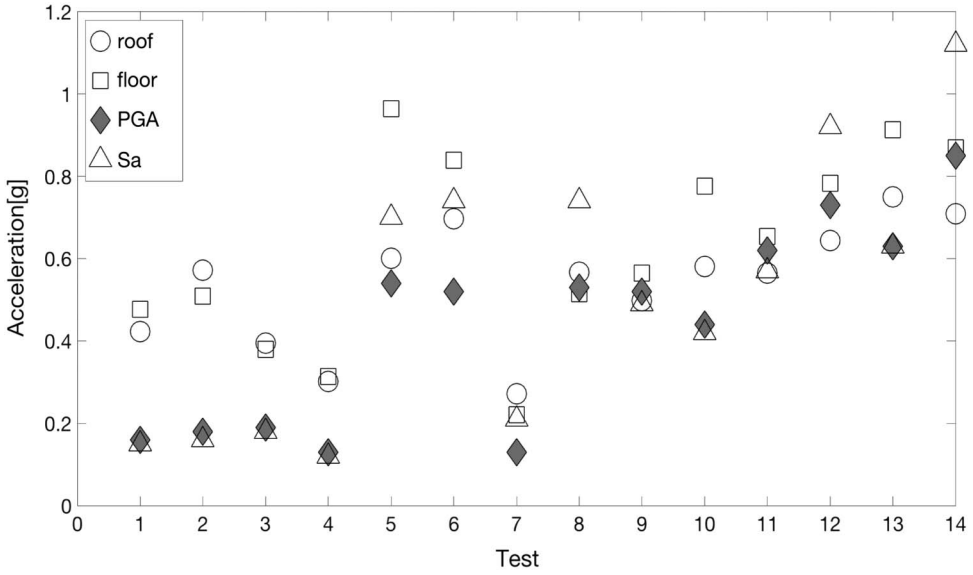

Fig. 14. Peak floor and roof acceleration (average from all sensors) compared to PGA and Sa at 0.9 s.

This value should be equal to the overall building drift if the rocking wall truly behaved as a rigid body. The resulting drift values are not the same and, as expected, the rigid body drift values are smaller than the true drifts. This indicates that a rigid block rocking at the toe is only a rough approximation for the behavior of the panels. The actual building drift will be larger because (1) the center of rotation of the panel is not exactly at the toe of the panel; (2) the panel itself can deform elastically and add to overall building deformation; and (3) there may potentially be gaps and additional deformation generated at the connections between the wall panels and the diaphragms.

Diaphragm Response

The diaphragms were designed to remain elastic during most of the ground motions. Although there was very limited deformation (maximum measured deflection at the roof diaphragm in Test 14 was only 24 mm over a 17.7-m diaphragm span) that developed during the tests, the diaphragms did not experience significant damage from seismic loading. Point-in-time diaphragm displacements at the time of peak roof drift for selected ground motions at the three different intensity levels are shown in Fig. 18. The deformation of the diaphragm can be seen from the measured absolute displacements of the three points on the diaphragm shown in the figure. As depicted, there was some diaphragm deformation at both the floor and roof that increased with increasing earthquake intensity. However, the deformation of the diaphragms was much less than the lateral drift of the lateral force-resisting system. The response of the diaphragm demonstrated that the CLT diaphragm can be designed and detailed to behave in a fairly rigid manner relative to the CLT rocking-wall lateral system. A rigid diaphragm assumption is likely adequate for this particular design configuration.

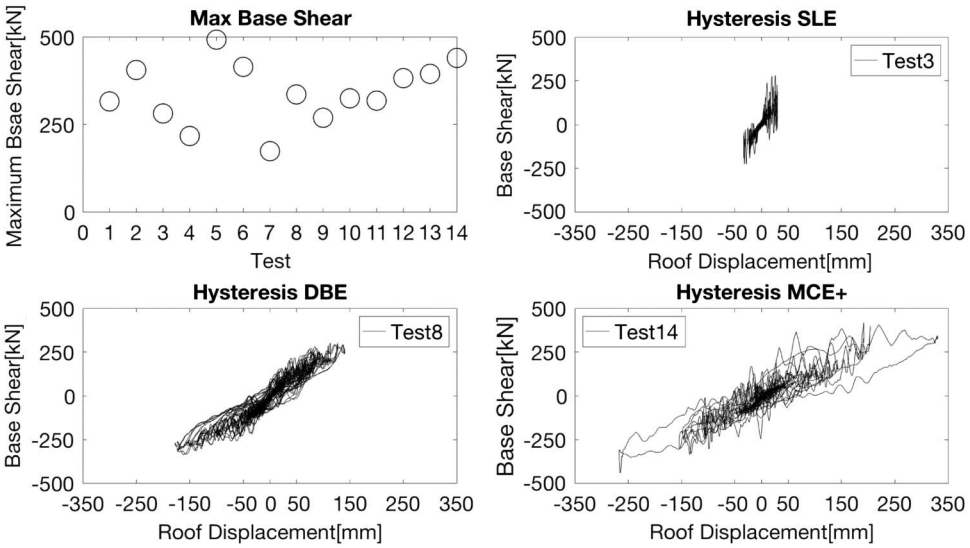

Fig. 15. Building peak base shear and example hysteresis loops.

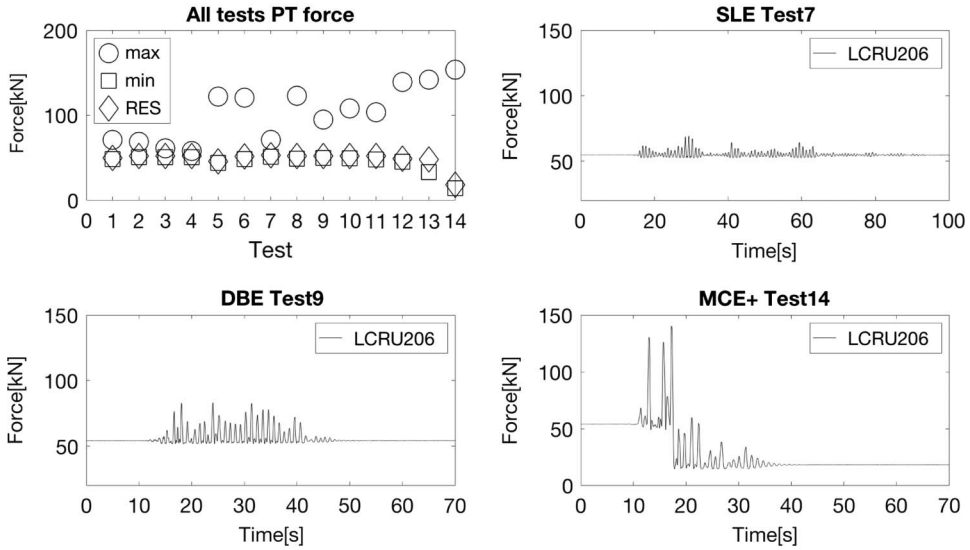

Fig. 16. Maximum/minimum post-tension rod forces and example force time history.

The force transfer between the rocking walls and the diaphragms was measured using strain gauges on the steel shear keys. The strain gauges were oriented 45° relative to the shear key center line in order to capture the maximum shear strain in the shear key cross section, assuming no normal strain at the gauge location. Using the cross-sectional properties of the shear keys, this measured strain can be used to estimate the shear force transferred from the diaphragm to the walls by assuming a parabolic distribution of shear strain. This approximation is notably coarse, but nonetheless provides useful insight into the distribution of shear forces at different shear key locations. For verification, the calculated shear key forces on a story can be summed and compared to the floor accelerations times the floor mass. The peak forces in the keys for all 14 tests are plotted in Fig. 19. These forces are the peak values at each location and do not necessarily occur at the same time. The shear demand distribution among the shear keys was not uniform. In large earthquakes, some shear keys seemed to resist close to 200% of shear force compared to other keys on the same level. The shear force at certain locations was also consistently larger than that at other locations, that is, the southwest shear key on both the floor and roof appeared to consistently transfer larger forces. This condition may be attributed to differences in the alignment of the shear key connections and the tolerances at the bearing location between the shear keys and slot in the wall panels. Such variability should be accounted for when designing the shear transfer details of the CLT rocking walls. Fig. 19 also shows the estimated shear key forces calculated from the story seismic force (maximum average story acceleration times the story mass) divided by four (i.e., assuming a uniform distribution) and labeled as "Story Force/4." The maximum shear force calculated based on strain gauge measurements does not exactly match that calculated based on acceleration measurements. This discrepancy is likely due to the data quality and the simplified shear force calculation. Fig. 20 provides a more direct visualization of this nonuniform shear force distribution using three example

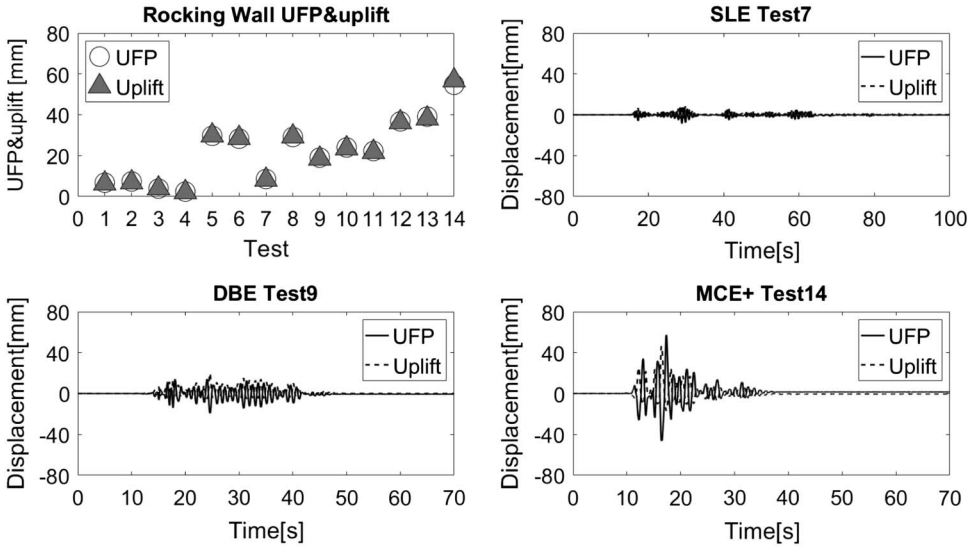

Fig. 17. Peak rocking-wall corner uplift and UFP deformation with example time history.

Table 2. Peak rocking-wall corner uplift and UFP deformation compared to peak building drift ratio

Test	Uplift (mm)	UFP (mm)	Uplift/B[a] %	UFP/B %	Roof displacement/H[a] (%)
1	6	6	0.41	0.36	0.78
2	7	6	0.45	0.40	0.81
3	4	3	0.26	0.23	0.50
4	2	2	0.13	0.12	0.39
5	30	26	1.96	1.72	2.63
6	29	25	1.88	1.65	2.54
7	8	7	0.54	0.47	0.83
8	29	26	1.93	1.70	2.63
9	18	16	1.21	1.07	1.65
10	24	21	1.54	1.36	2.12
11	22	19	1.43	1.26	1.93
12	36	32	2.38	2.10	3.27
13	38	34	2.50	2.20	3.28
14	57	50	3.73	3.28	5.07

[a]Width of the CLT wall panel B = Height of the roof H = 6.71 m (22 ft).

tests, with all maximum forces normalized by the maximum shear force measured during the DBE level test at the southwest key location.

Damage Observation

The specimen was inspected for damage after each test at the DBE or MCE level. Because the structural system was designed to achieve a resilient performance objective, there was no significant damage to the building at any time during the entire testing program. The post-tensioned rocking walls were able to recenter the building even when some of the MCE level motions caused post-tension loss in the PT rods. The glulam beam-to-column joints performed very well during dynamic testing and showed no visible damage after 14 ground motions. The diaphragm remained essentially elastic and rigid with no signs of permanent slip or deformation. The only visible damage was found at the bottom corners of the rocking-wall panels after large DBE and MCE ground motions. The damage was not significant enough to warrant structural repair (e.g., splitting of the outside wood fiber and slight deformation of the toe). These damage patterns were identical to those observed in previous cyclic tests conducted on rocking-wall components at similar drift levels (Ganey et al. 2017). After all 14 earthquakes were completed, the rocking walls were disassembled and taken out of the building for examination. The typical damage at the rocking-wall toe is shown in Fig. 21. The damage to the wall only minimally affected the rocking-wall performance, but not to the degree that repair would be needed. The building was intentionally pushed to very large drift levels, beyond what is required by current building codes. At the code-specified drift levels, the structural system was essentially damage free.

Conclusions

The test program summarized herein represents the first full-scale shake table test of a mass-timber building with an open floor plan and a resilient lateral system. The resilient performance goal of no major structural damage was achieved in all tests. Although the current test structure was only two stories, subsequent research and development in the NHERI Tall Wood Project will further advance these prototype systems and concepts to taller building configurations. The following specific conclusions can be drawn based on direct observation of the test building performance presented in this study.

1. It is possible to combine a CLT rocking-wall system with a heavy-timber gravity system to achieve a resilient performance under repeated earthquakes at DBE and MCE intensity levels, provided the appropriate details were implemented to (1) decouple the vertical movement of the rocking walls and horizontal movement of the diaphragm, and (2) accommodate gravity-system deformation compatibility.
2. During the entire experimental program of 14 tests, only 2 MCE level tests resulted in the need to retension the PT bars. The lateral design of the building was intended to require no repair for SLE and DBE level tests, and relatively easy repair (retension of the PT bars) for the MCE level tests. This objective was achieved based on the measured data, indicating the resilience of the rocking-wall system in DBE-level earthquakes (i.e., no structural repair required).
3. By using relatively simple panel connection details and readily available fasteners, CLT diaphragms can be designed to essentially behave in a rigid manner under large earthquakes.

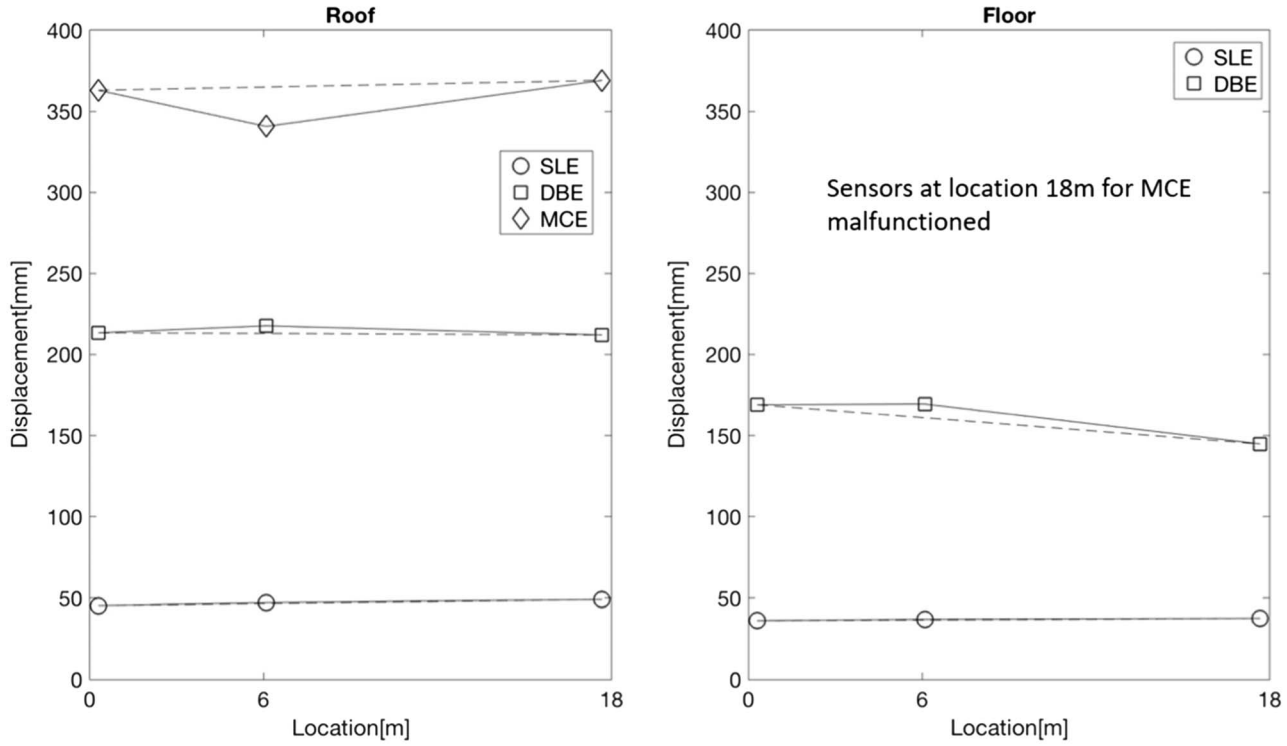

Fig. 18. Absolute displacement from three points on the diaphragms at the peak displacement time point.

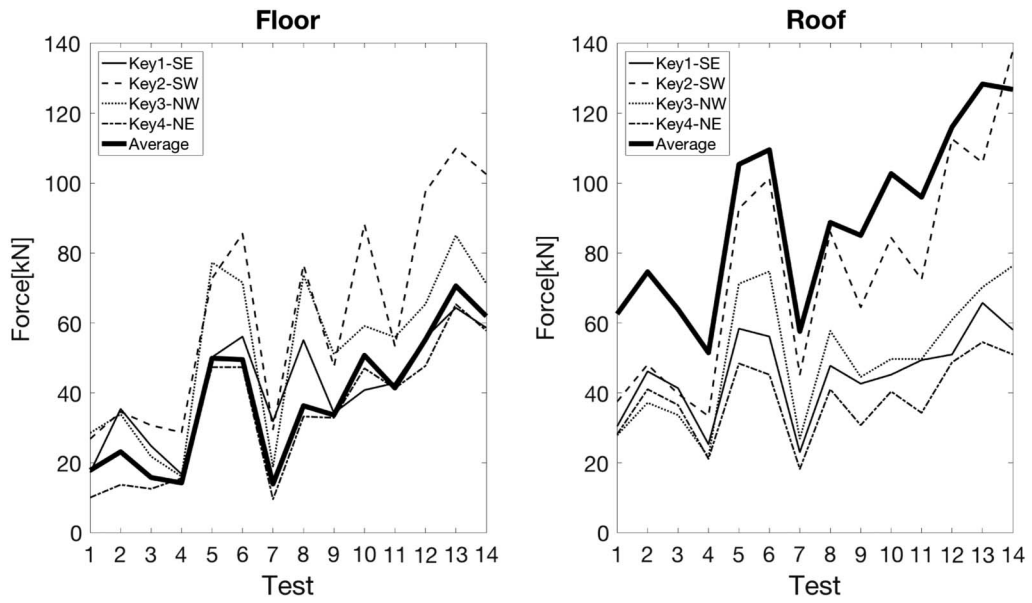

Fig. 19. Peak shear key force estimation from all seismic tests.

The reduction in diaphragm force demand through the use of a flexible rocking-wall system can contribute to an improved diaphragm performance.

4. The shear transfer between the diaphragm and rocking wall is critical for the proposed lateral system. The nonuniform distribution of the shear demand among the shear key detail must be considered in the design or appropriate detailing to ensure equal load sharing pursued. The use of an overstrength factor or capacity design for such details is recommended. A more detailed investigation on the load-sharing characteristics of multiple rocking-wall shear keys within a CLT diaphragm should be conducted in future research efforts.
5. The shear transfer detail used in this test program to transfer the shear load from the key to the diaphragm was effective: it was constructible and allowed for the intended rocking response of the wall.

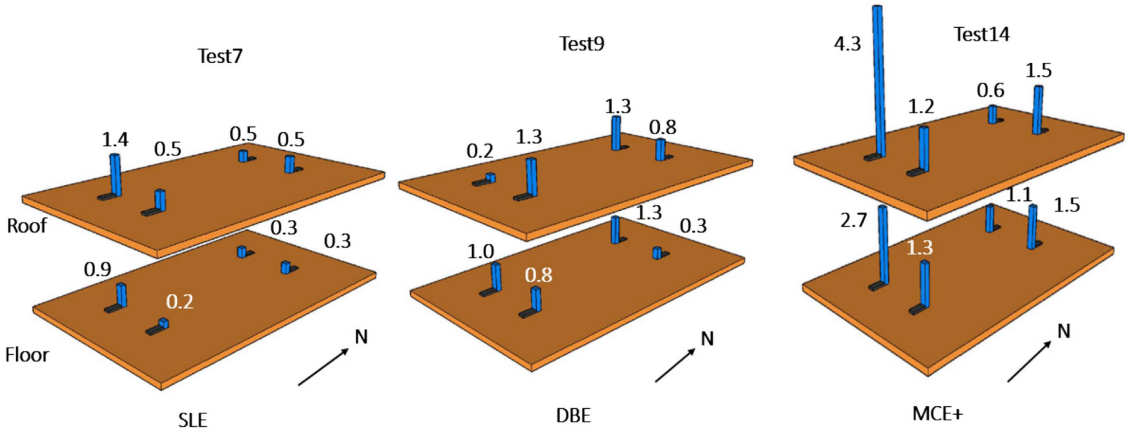

Fig. 20. Example uneven distribution of the shear key forces at different intensity levels, normalized by peak southwest floor shear key force at the DBE event.

Slight compression deformation at the rocking wall corner

Chipping of wood at the rocking wall corner

Fig. 21. Very limited and localized damage observed at rocking-wall corners.

6. The gravity connection details used in this test program can tolerate a very large (up to 5%) interstory drift without inducing damage or the loss of stability.
7. The natural period of the test building is relatively long for the given building height. Stiffness and deformation are likely to control the design for taller building implementations.

Acknowledgments

This research project is supported by the National Science Foundation through a number of collaborative awards, including CMMI 1636164, CMMI 1634204, CMMI 1635363, CMMI 1635227, CMMI 1635156, and CMMI 1634628. The use of the NHERI experimental facility is supported by the National Science Foundation's Natural Hazards Engineering Research Infrastructure (NHERI) Program. The authors would like to thank the NHERI at UCSD site management and staff, who helped greatly in the construction and testing program. The authors would also like to acknowledge support for the 2-story shake table testing program from industry partners, including TallWood Design Institute, Katerra, Simpson Strong-Tie, Forest Products Laboratory, Softwood Lumber Board, DR Johnson Lumber, and the City of Springfield, Oregon. The opinions presented herein are solely those of the authors. The authors also would like to acknowledge individual industry collaborators and students who worked on this project, including Jace Furley, Leonardo Rodrigues, Brian Demeza, Gabriele Tamagnone, Daniel Griesenauer, Ethan Judy, Steven Kordziel, Aleesha Busch, Ali Hansan, Joycelyn Ng, Monica Y. Liu, and Ata Mohseni. The authors would also like to thank the NHERI TallWood project Co-PIs (Keri Ryan at University of Nevada Reno, James Ricles and Richard Sause at Lehigh University).

References

Akbas, T., et al. 2017. "Analytical and experimental lateral-load response of self-centering posttensioned CLT walls." *J. Struct. Eng.* 143 (6): 04017019. https://doi.org/10.1061/(ASCE)ST.1943-541X.0001733.

APA—The Engineered Wood Association. 2018a. *Product report: DRJ cross-laminated timber.* PR-L320. Tacoma, WA: APA—The Engineered Wood Association.

APA—The Engineered Wood Association. 2018b. *Standard for performance-rated cross laminated timber.* ANSI/APA PRG 320. Tacoma, WA: APA—The Engineered Wood Association.

ASCE. 2010. *Minimum design loads and associated criteria for buildings and other structures.* ASCE/SEI 7-10. Reston, VA: ASCE.

Buchanan, A., B. Deam, M. Fragiacomo, S. Pampanin, and A. Palermo. 2008. "Multi-storey prestressed timber buildings in New Zealand." *Struct. Eng. Int.* 18 (2): 166–173. https://doi.org/10.2749/101686608784218635.

Building Code Division, State of Oregon. 2018. *Statewide alternative method No. 18-01 tall wood buildings*. Salem, OR: Oregon Building Code Division.

Ceccotti, A., C. Sandhaas, M. Okabe, M. Yasumura, C. Minowa, and N. Kawai. 2013. "SOFIE project–3D shaking table test on a seven-storey full-scale cross-laminated timber building." *Earthquake Eng. Struct. Dyn.* 42 (13): 2003–2021. https://doi.org/10.1002/eqe.2309.

Ganey, R., et al. 2017. "Experimental investigation of self-centering cross-laminated timber walls." *J. Struct. Eng.* 143 (10): 04017135. https://doi.org/10.1061/(ASCE)ST.1943-541X.0001877.

Higgins, C., A. R. Barbosa, and C. Blank. 2017. *Structural tests of composite concrete-cross-laminated timber floors*. Research Rep. No. 17-01. Corvallis, OR: Oregon State Univ.

Holden, A., C. Devereux, S. Haydon, A. Buchanan, and S. Pampanin. 2012. "Innovative structural design of a three storey post-tensioned timber building." In *Proc., World Conf. on Timber Engineering, Architecture and Engineering Case Studies*, 323–330. Auckland, New Zealand: WCTE 2012 Local Organization Committee.

ICC-Evaluation Service. 2018. *ICC-ES evaluation report: ESR-3178*. Washington, DC: ICC Evaluation Service.

Iqbal, A., S. Pampanin, and A. H. Buchanan. 2016a. "Seismic performance of full-scale post-tensioned timber beam-column joints." *J. Earthquake Eng.* 20 (3): 383–405. https://doi.org/10.1080/13632469.2015.1070386.

Iqbal, A., S. Pampanin, A. Palermo, and A. H. Buchanan. 2015. "Performance and design of LVL walls coupled with UFP dissipaters." *J. Earthquake Eng.* 19 (3): 383–409. https://doi.org/10.1080/13632469.2014.987406.

Iqbal, A., T. Smith, S. Pampanin, M. Fragiacomo, A. Palermo, and A. H. Buchanan. 2016b. "Experimental performance and structural analysis of plywood-coupled LVL walls." *J. Struct. Eng.* 142 (2): 04015123. https://doi.org/10.1061/(ASCE)ST.1943-541X.0001383.

Johnson, B. 2017. *Timber tower research project—SOM: Physical testing report #1, composite timber floor testing at Oregon State University*. Accessed August 5, 2018. https://www.som.com/FILE/27750/2017_timber_tower_som_osu_report.pdf.

Johnston, H., C. Watson, S. Pampanin, and A. Palermo. 2014. "Shake table testing of an integrated low damage building system." In *Proc., 2nd European Conf. in Earthquake Engineering and Seismology*, 25–29. Oakland, CA: Earthquake Engineering Research Institute.

Palermo, A., S. Pampanin, A. Buchanan, and M. Newcombe. 2005. *Seismic design of multi-storey buildings using laminated veneer lumber (LVL)*. Christchurch, New Zealand: Univ. of Canterbury Research Repository.

Palermo, A., S. Pampanin, M. Fragiacomo, A. H. Buchanan, and B. L. Deam. 2006. *Innovative seismic solutions for multi-storey LVL timber buildings*. Christchurch, New Zealand: Univ. of Canterbury Research Repository.

Palermo, A., F. Sarti, A. Baird, D. Bonardi, D. Dekker, and S. Chung. 2012. "From theory to practice: Design, analysis and construction of dissipative timber rocking post-tensioning wall system for Carterton Events Centre, New Zealand." In *Proc., 15th World Conf. on Earthquake Engineering*, 24–28. Lisbon, Portugal: WCEE2012 Local Organization Committee.

Pei, S., J. W. van de Lindt, A. R. Barbosa, J. W. Berman, H.-E. Blomgren, J. Dolan, E. McDonnell, R. Zimmerman, M. Fragiacomo, D. Rammer. 2018. "Full-scale shake table test of a two-story mass-timber building with resilient rocking walls." In *Proc., 16th European Conf. on Earthquake Engineering*. Thessaloniki, Greece: 16ECEE Local Organization Committee.

Pei, S., J. W. Van De Lindt, M. Popovski, J. W. Berman, J. D. Dolan, J. Ricles, R. Sause, H. Blomgren, and D. R. Rammer. 2014. "Cross-laminated timber for seismic regions: Progress and challenges for research and implementation." *J. Struct. Eng.* 142 (4): E2514001. https://doi.org/10.1061/(ASCE)ST.1943-541X.0001192.

Popovski, M., J. Schneider, and M. Schweinsteiger. 2010. "Lateral load resistance of cross-laminated wood panels." In *Proc., World Conf. on Timber Engineering*, 20–24. Rome, Italy: National Research Council of Italy, Trees and Timber Institute.

Priestley, M. N., S. Sritharan, J. R. Conley, and S. Pampanin. 1999. "Preliminary results and conclusions from the PRESSS five-story precast concrete test building." *PCI J.* 44 (6): 42–67. https://doi.org/10.15554/pcij.11011999.42.67.

Sause, R., J. M. Ricles, D. A. Roke, N. B. Chancellor, and N. P. Gonner. 2010. "Seismic performance of a self-centering rocking concentrically-braced frame." In *Proc., 9th US National and 10th Canadian Conf. on Earthquake Engineering*, 25–29. Oakland, CA: Earthquake Engineering Research Institute.

van de Lindt, J. W., P. Bahmani, G. Mochizuki, S. E. Pryor, M. Gershfeld, J. Tian, D. Rammer, and M. D. Symans. 2013. "Experimental seismic behavior of a full-scale four-story soft-story woodframe building II: Shake table test results." *J. Struct. Eng.* 142 (4): E4014004. https://doi.org/10.1061/(ASCE)ST.1943-541X.0001206.

van de Lindt, J. W., S. Pei, S. E. Pryor, H. Shimizu, and H. Isoda. 2010. "Experimental seismic response of a full-scale six-story light-frame wood building." *J. Struct. Eng.* 136 (10): 1262–1272. https://doi.org/10.1061/(ASCE)ST.1943-541X.0000222.

Zimmerman, R. B., and E. McDonnell. 2018. "Framework—Innovation in re-centering mass timber wall buildings." In *Proc., 11th National Conf. in Earthquake Engineering*. Los Angeles, CA: Earthquake Engineering Research Institute.